

Constructing Metrics of Consistency from EOP Combined Series: An Example Applied to ITRF2014, JTRF2014, and DTRF2014

Claudio Abbondanza¹, Toshio M Chin¹, Richard S Gross¹,
Michael B Heflin¹, Jay W Parker¹, Benedikt S Soja¹,
Xiaoping Wu¹,

December 13, 2018

¹ Jet Propulsion Laboratory - California Institute of Technology



Jet Propulsion Laboratory
California Institute of Technology

Introduction

Motivation and Overview

- Effort to assess the quality of TRF-derived EOP series (ITRF2014, JTRF2104, DTRF2014) via
 - **intra-comparisons** of the the series to JPL Earth Orientation Products such as COMB2016 (Ratcliff and Gross, 2017)
 - **inter-comparisons** to models of geophysical Effective Angular Momentum (EAM) (Barnes *et al.*, 1983), aka **excitation functions**.
- **Intra-comparisons** (time domain) point out the existence of **systematic effects** in the EOP series mostly related to the different combination schemes, data editing, weighting approaches etc.
- **Inter-comparisons** (mainly through spectral methods) aim to assess the degree of consistency between the observed **Geodetic** and **Geophysical** excitations.
 - In principle, the approach is successful if the EAM geophysical excitations were significantly more accurate than the observed ones (Rebischung *et al.*, 2017).

Intra-Comparisons and Internal Consistency among the Earth Orientation Series

- Multi-Technique Space Geodesy Earth Orientation Series
 - EOPs & TRFs simultaneously adjusted
 - (\mathcal{I}) ITRF2014 (Altamimi *et al.*, 2016)
 - (\mathcal{J}) JTRF2014
 - (\mathcal{D}) DTRF2014 (Seitz *et al.*, 2016)
 - EOPs calibrated in isolation via Kalman Filtering (Gross *et al.*, 1998)
 - (\mathcal{C}) COMB2016 (Ratcliff and Gross, 2017)
- Geophysical Earth Effective Angular Momentum Functions (EAMFs)
 - GFZ EAMFs (Dobslaw and Dill, 2018)
 - Atmosphere
 - Oceans
 - Land Water (Continental Water Surface)
 - Sea-Level (Mass-Conserving Layer)

Space Geodesy Earth Orientation Series (comb TRFs)

EOP	TRF	GNSS (P)	VLBI (R)	SLR (L)	DORIS (D)	LLR
(x_p, y_p)	ITRF	•	•	•	•	•
	JTRF	•	•	•	•	•
	DTRF	•	•	•	•	•
	COMB		•	•	•	
UT	ITRF	•		•		
	JTRF	•		•		
	DTRF	•		•		
	COMB			•		•
(\dot{x}_p, \dot{y}_p)	ITRF	•	•	•		
	JTRF	•	•	•		
	DTRF	•	•	•		
	COMB					
LOD	ITRF	•		•		
	JTRF	•		•		
	DTRF	•	•	•	•	
	COMB		•			
(VOL, UT)	ITRF					
	JTRF					
	DTRF					
	COMB					•

Observational contributions to combined (multi-technique) Earth Orientation Parameters for the three TRF products and COMB2016. Bulleted cells in the double-entry table indicate which of the EOP parameters observed by which of the space-geodetic and astrometric techniques were used. P stands for GNSS, R is VLBI, L SLR, and D DORIS. LLR stands for Lunar Laser Ranging, ILS International Latitude Service providing astrometric observations of polar motion and UT1, VOL Variation of Latitude.

Space Geodesy Earth Orientation Series (COMB2016)

EOP		TRF	GNSS (P)	VLBI (R)	SLR (L)	DORIS (D)	LLR
(x_p, y_p)	ITRF	•	•	•	•	•	
	JTRF	•	•	•	•	•	
	DTRF	•	•	•	•	•	
	COMB		•	•	•		
UT	ITRF	•		•			
	JTRF	•		•			
	DTRF	•		•			
	COMB			•			•
(\dot{x}_p, \dot{y}_p)	ITRF	•	•	•			
	JTRF	•	•	•			
	DTRF	•	•	•			
	COMB						
LOD	ITRF	•		•			
	JTRF	•		•			
	DTRF	•	•	•	•		
	COMB		•				
(VOL, UT)	ITRF						
	JTRF						
	DTRF						
	COMB						•

Observational contributions to combined (multi-technique) Earth Orientation Parameters for the three TRF products and COMB2016. Bulleted cells in the double-entry table indicate which of the EOP parameters observed by which of the space-geodetic and astrometric techniques were used. P stands for GNSS, R is VLBI, L SLR, and D DORIS. LLR stands for Lunar Laser Ranging, VOL Variation of Latitude.

EOP differences to JPL-COMB2016 - Biases and Trends

		<i>Bias</i>	<i>Rate</i>	<i>Annual</i>	<i>Semi</i>	<i>RMS</i>
x_p	ITRF	3.86 (0.68)	-0.85 (0.14)	9.27 (0.82)	1.06 (0.81)	51.13
	JTRF	32.89 (0.73)	-4.11 (0.16)	8.02 (0.79)	4.50 (0.77)	48.67
	DTRF	-17.16 (5.52)	5.90 (1.06)	6.62 (1.09)	8.83 (1.04)	52.46
y_p	ITRF	2.40 (0.58)	-1.44 (0.12)	1.17 (0.72)	4.95 (0.71)	44.83
	JTRF	25.96 (0.64)	2.79 (0.14)	18.36 (0.69)	6.74 (0.67)	43.54
	DTRF	-3.89 (5.31)	1.34 (1.01)	8.29 (1.05)	9.12 (1.01)	43.89
UT	ITRF	-0.18 (0.16)	0.07 (0.03)	1.03 (0.25)	0.76 (0.25)	16.31
	JTRF	-2.81 (0.17)	0.37 (0.03)	0.96 (0.25)	0.78 (0.26)	15.66
	DTRF	-2.62 (4.40)	0.28 (0.85)	0.49 (0.36)	0.13 (0.36)	12.47
\dot{x}_p	ITRF	28.86 (2.16)	6.11 (0.42)	58.88 (2.24)	16.29 (2.24)	126.25
	JTRF	27.80 (2.25)	6.23 (0.44)	56.53 (2.20)	14.34 (2.20)	125.14
	DTRF	26.71 (4.55)	5.98 (0.90)	59.81 (2.93)	10.58 (2.94)	171.31
\dot{y}_p	ITRF	17.25 (2.12)	9.26 (0.41)	69.45 (2.75)	7.92 (2.75)	154.94
	JTRF	17.96 (2.21)	9.14 (0.43)	69.30 (2.67)	9.04 (2.66)	151.65
	DTRF	20.01 (4.46)	9.68 (0.89)	77.76 (3.26)	3.32 (3.27)	190.66
LOD	ITRF	-0.47 (0.35)	0.10 (0.07)	2.26 (1.28)	2.07 (1.28)	54.45
	JTRF	-0.56 (0.35)	0.12 (0.07)	2.21 (1.28)	2.01 (1.28)	53.78
	DTRF	5.07 (3.55)	-0.18 (0.71)	4.89 (3.99)	4.10 (4.09)	135.74

Least-square fits of the EOP differences to COMB to the model $h(t) = a + b \cdot (t - t_0) + c \cdot \sin[\omega(t - t_0) - \varphi]$, where h is the generic Earth Orientation parameter, The reference epoch t_0 is set to January 1 2005. Units are μas for polar motion components and $\mu\text{as}/d$ for polar motion rate. UT and LOD are expressed in $\mu\text{as}/\text{day}$. The RMS's reported in the last column are computed after the removal of linear trends and seasonal terms and expressed in μas and $\mu\text{as}/\text{day}$. TCH estimates shown here are based on Earth orientation time series spanning the time window 1998.0-2015.0. None of the systematic effects affecting the individual series (biases, trends, seasonals) was removed prior to performing TCH.

EOP differences to JPL-COMB2016 - Seasonals

		<i>Bias</i>	<i>Rate</i>	<i>Annual</i>	<i>Semi</i>	<i>RMS</i>
x_p	ITRF	3.86 (0.68)	-0.85 (0.14)	9.27 (0.82)	1.06 (0.81)	51.13
	JTRF	32.89 (0.73)	-4.11 (0.16)	8.02 (0.79)	4.50 (0.77)	48.67
	DTRF	-17.16 (5.52)	5.90 (1.06)	6.62 (1.09)	8.83 (1.04)	52.46
y_p	ITRF	2.40 (0.58)	-1.44 (0.12)	1.17 (0.72)	4.95 (0.71)	44.83
	JTRF	25.96 (0.64)	2.79 (0.14)	18.36 (0.69)	6.74 (0.67)	43.54
	DTRF	-3.89 (5.31)	1.34 (1.01)	8.29 (1.05)	9.12 (1.01)	43.89
UT	ITRF	-0.18 (0.16)	0.07 (0.03)	1.03 (0.25)	0.76 (0.25)	16.31
	JTRF	-2.81 (0.17)	0.37 (0.03)	0.96 (0.25)	0.78 (0.26)	15.66
	DTRF	-2.62 (4.40)	0.28 (0.85)	0.49 (0.36)	0.13 (0.36)	12.47
\dot{x}_p	ITRF	28.86 (2.16)	6.11 (0.42)	58.88 (2.24)	16.29 (2.24)	126.25
	JTRF	27.80 (2.25)	6.23 (0.44)	56.53 (2.20)	14.34 (2.20)	125.14
	DTRF	26.71 (4.55)	5.98 (0.90)	59.81 (2.93)	10.58 (2.94)	171.31
\dot{y}_p	ITRF	17.25 (2.12)	9.26 (0.41)	69.45 (2.75)	7.92 (2.75)	154.94
	JTRF	17.96 (2.21)	9.14 (0.43)	69.30 (2.67)	9.04 (2.66)	151.65
	DTRF	20.01 (4.46)	9.68 (0.89)	77.76 (3.26)	3.32 (3.27)	190.66
LOD	ITRF	-0.47 (0.35)	0.10 (0.07)	2.26 (1.28)	2.07 (1.28)	54.45
	JTRF	-0.56 (0.35)	0.12 (0.07)	2.21 (1.28)	2.01 (1.28)	53.78
	DTRF	5.07 (3.55)	-0.18 (0.71)	4.89 (3.99)	4.10 (4.09)	135.74

Least-square fits of the EOP differences to COMB to the model $h(t) = a + b \cdot (t - t_0) + c \cdot \sin[\omega(t - t_0) - \varphi]$, where h is the generic Earth Orientation parameter, The reference epoch t_0 is set to January 1 2005. Units are μas for polar motion components and $\mu\text{as}/d$ for polar motion rate. UT and LOD are expressed in $\mu\text{s}/\text{day}$. The RMS's reported in the last column are computed after the removal of linear trends and seasonal terms and expressed in μas and $\mu\text{as}/\text{day}$. TCH estimates shown here are based on Earth orientation time series spanning the time window 1998.0-2015.0.

EOP differences to JPL-COMB2016 - Seasonals

- Due to the Linear Coupling/Degeneracy between $(x_p, y_p, UT1)$ and rotational Helmert parameters,
- EOP corruption at seasonal frequencies may reflect inconsistencies in the way the TRF combinations are being conducted
 - **JTRF** In the combination, time series of GNSS rotational parameters R_1 (in particular) and R_2 are affected by anomalous seasonal signals and this, in turn, affects x_p and y_p (in particular)
 - **ITRF** In the stacking, seasonal terms are being fitted to the station position time series.
 - **DTRF** Daily/Weekly Non-tidal Atmospheric Loading Models are being removed from the station position time series (NTAL loading signal is the strongest at seasonal frequencies).
- This (we speculate) may affect rotations and, in turn, may produce inconsistencies in the combined polar motion

EOP differences to JPL-COMB2016 - RMSs

		<i>Bias</i>	<i>Rate</i>	<i>Annual</i>	<i>Semi</i>	<i>RMS</i>
x_p	ITRF	3.86 (0.68)	-0.85 (0.14)	9.27 (0.82)	1.06 (0.81)	51.13
	JTRF	32.89 (0.73)	-4.11 (0.16)	8.02 (0.79)	4.50 (0.77)	48.67
	DTRF	-17.16 (5.52)	5.90 (1.06)	6.62 (1.09)	8.83 (1.04)	52.46
y_p	ITRF	2.40 (0.58)	-1.44 (0.12)	1.17 (0.72)	4.95 (0.71)	44.83
	JTRF	25.96 (0.64)	2.79 (0.14)	18.36 (0.69)	6.74 (0.67)	43.54
	DTRF	-3.89 (5.31)	1.34 (1.01)	8.29 (1.05)	9.12 (1.01)	43.89
UT	ITRF	-0.18 (0.16)	0.07 (0.03)	1.03 (0.25)	0.76 (0.25)	16.31
	JTRF	-2.81 (0.17)	0.37 (0.03)	0.96 (0.25)	0.78 (0.26)	15.66
	DTRF	-2.62 (4.40)	0.28 (0.85)	0.49 (0.36)	0.13 (0.36)	12.47
\dot{x}_p	ITRF	28.86 (2.16)	6.11 (0.42)	58.88 (2.24)	16.29 (2.24)	126.25
	JTRF	27.80 (2.25)	6.23 (0.44)	56.53 (2.20)	14.34 (2.20)	125.14
	DTRF	26.71 (4.55)	5.98 (0.90)	59.81 (2.93)	10.58 (2.94)	171.31
\dot{y}_p	ITRF	17.25 (2.12)	9.26 (0.41)	69.45 (2.75)	7.92 (2.75)	154.94
	JTRF	17.96 (2.21)	9.14 (0.43)	69.30 (2.67)	9.04 (2.66)	151.65
	DTRF	20.01 (4.46)	9.68 (0.89)	77.76 (3.26)	3.32 (3.27)	190.66
LOD	ITRF	-0.47 (0.35)	0.10 (0.07)	2.26 (1.28)	2.07 (1.28)	54.45
	JTRF	-0.56 (0.35)	0.12 (0.07)	2.21 (1.28)	2.01 (1.28)	53.78
	DTRF	5.07 (3.55)	-0.18 (0.71)	4.89 (3.99)	4.10 (4.09)	135.74

Least-square fits of the EOP differences to COMB to the model $h(t) = a + b \cdot (t - t_0) + c \cdot \sin[\omega(t - t_0) - \varphi]$, where h is the generic Earth Orientation parameter, The reference epoch t_0 is set to January 1 2005. Units are μas for polar motion components and $\mu\text{as}/d$ for polar motion rate. UT and LOD are expressed in $\mu\text{s}/\text{day}$. The RMS's reported in the last column are computed after the removal of linear trends and seasonal terms and expressed in μas and $\mu\text{as}/\text{day}$. TCH estimates shown here are based on Earth orientation time series spanning the time window 1998.0-2015.0.

Three-Corner Hat Estimates of the EOP Uncertainties

- **Model** $x_i = s + \varepsilon_i$ (Premoli and Tavella, 1993)
- No stochastic assumption made on ε , whose estimates may be affected by the time-correlated (red) background noise.

	x_p (uas)	y_p (uas)	UT (us)	\dot{x}_p (uas/d)	\dot{y}_p (uas/d)	LOD (us/d)
ITRF	18.66	19.93	7.21	11.87	12.13	9.32
JTRF	26.74	23.15	5.50	12.98	14.21	10.06
DTRF	30.23	14.15	14.30	116.74	116.80	142.26
<i>OBS</i>	6212	6212	2323	6208	6208	2323

TCH-based estimates of the uncertainty (i.e. square-root of the variance associated with the process noise) characterizing the 3 Earth Orientation time series from ITRF, DTRF, and JTRF. The last row reports the number of common observations per EOP used in the estimation process. Values reported in the Table are standard deviations whose units are μas for the pole coordinates, $\mu s/d$ for UT and LOD and $\mu as/d$ for polar motion rates. TCH estimates shown here are based on Earth orientation time series spanning the time window 1998.0-2015.0.

Parametric Spectral Estimates of PM Background Noise

Let's make some assumption on the polar motion (PM) noise structure

- **First-order Autoregressive AR[1] (time domain) Model**

$$p_t = \varphi p_{t-1} + \varepsilon_t, \quad \varepsilon \sim \mathcal{N}(0, \sigma^2)$$

where

p and ε are complex-valued PM and Gaussian noise (std σ)

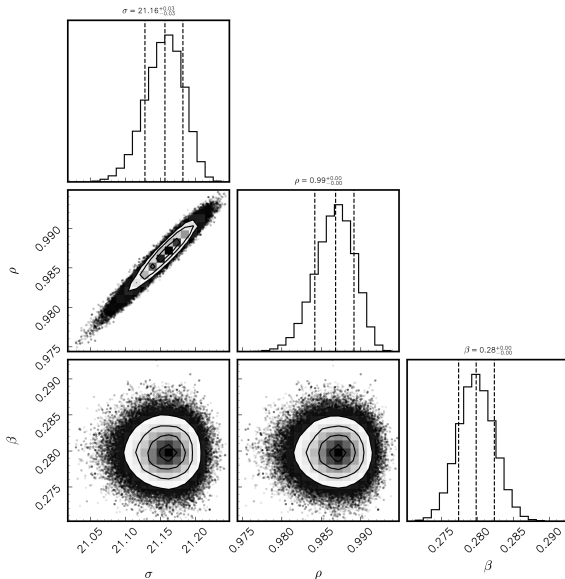
φ is the lag-one autocorrelation of the process $\in [-1, 1]$

- **AR[1] Spectral Domain Representation** (see e.g. Brockwell, P. J. and Davis, R. A., 1986)

$$S_p(\omega) = \frac{\sigma^2}{2\pi} \frac{1}{|1 - \varphi e^{-i\omega}|^2}$$

- (σ, φ) obtained via **Bayesian Inversion** of the adaptive multi-tapered empirical spectrum $\tilde{S}_p(\omega)$

Bayesian Inversion - Sampled Posterior Distributions



Bayesian Inversion - Median Estimates of (σ, ϕ)

- $\phi \sim 1.0$ indicates PM background noise consistent with **random walk**
- σ is an estimate of the **high-frequency** (close to the Nyquist, i.e. 0.5 cpd) noise level

	σ (μas)	ϕ
COMB	22.1406 (-0.0029,0.0024)	0.9869 (-0.0323,0.0275)
ITRF	21.1565 (-0.0027,0.0023)	0.9868 (-0.0297,0.0259)
JTRF	20.9212 (-0.0027,0.0023)	0.9869 (-0.0295,0.0254)
DTRF	17.9566 (-0.0031,0.0026)	0.9881 (-0.0288,0.0246)

The estimates reported are median values sampled from the posterior distribution. Parenthesized are 15.73-th and 84-th percentiles, respectively. Units for σ are μas . ϕ is dimensionless.

Inter-Comparisons and Consistency among observed and GFZ-modelled excitation series

- Multi-Technique Space Geodesy Earth Orientation Series
 - \mathcal{C} COMB2016 (Ratcliff and Gross, 2017)
 - \mathcal{I} ITRF2014 (Altamimi *et al.*, 2016)
 - \mathcal{J} JTRF2014
 - \mathcal{D} DTRF2014 (Seitz *et al.*, 2016)
- Geophysical Earth Effective Angular Momentum Functions (EAMFs)
 - GFZ EAMFs (Dobslaw and Dill, 2018)
 - Atmosphere
 - Oceans
 - Land Water (Continental Water Surface)
 - Sea-Level (Mass-Conserving Layer)

Constructing Excitations from PM Observations $\tilde{\rho}$

- (a) **Time Deconvolution** (see e.g. Wilson, 1985; Wilson and Chen, 1996)

$$\tilde{\chi}(t) = \frac{ie^{-\frac{i\pi\Delta T}{T_{cw}}}}{\sigma_{cw}\Delta T} \left[\tilde{\rho}\left(t + \frac{\Delta T}{2}\right) - e^{i\pi\sigma_{cw}\Delta T} \tilde{\rho}\left(t - \frac{\Delta T}{2}\right) \right]$$

Please, note that polar motion rates are not involved here

- (b) If **polar motion rates observations** are available (see e.g. Kouba, 2005; Ray *et al.*, 2005)

$$\tilde{\chi}(t) = \tilde{\rho}(t) + \frac{i}{\sigma_{cw}} \frac{d}{dt} \tilde{\rho}(t)$$

- Comparing (a) and (b) to modelled EAM functions may provide some insight on the quality of the observed PM rates.

**Comparing observed and
GFZ-modelled χ at seasonal
frequencies**

Seasonals - Observed (Wilson and Chen, 1996) vs GFZ $\tilde{\chi}$

- No PM rate observations have been used to construct the observed $\tilde{\chi}$

	Annual				Semi-Annual			
	Prograde		Retrograde		Prograde		Retrograde	
	A (uas)	φ (deg)	A (uas)	φ (deg)	A (uas)	φ (deg)	A (uas)	φ (deg)
Observed Excitation (1998.0-2015.0)								
<i>C</i>	17591.2 (405.2)	114.2 (1.3)	10820.8 (405.2)	52.3 (1.8)	2863.4 (405.1)	106.2 (8.1)	4088.8 (405.1)	124.3 (7.6)
<i>I</i>	17588.2 (413.1)	114.2 (1.3)	10814.3 (413.1)	52.3 (1.8)	2866.1 (412.9)	106.2 (8.3)	4076.1 (412.9)	124.3 (7.7)
<i>J</i>	17587.8 (412.9)	114.2 (1.3)	10834.6 (413.0)	52.4 (1.8)	2860.6 (412.8)	106.2 (8.3)	4077.8 (412.8)	124.1 (7.7)
<i>D</i>	17588.7 (413.3)	114.2 (1.3)	10821.9 (413.3)	52.3 (1.8)	2866.6 (413.2)	106.2 (8.3)	4077.7 (413.2)	124.2 (7.7)
Total Geophysical Excitation (1998.0-2015.0)								
<i>T</i>	17378.5 (448.0)	116.6 (1.5)	8762.3 (448.0)	59.3 (2.2)	823.1 (447.8)	106.4 (31.2)	1559.5 (447.8)	171.3 (29.2)

Amplitudes are in *uas* (microarcseconds) and phases are given in decimal degrees. The reference epoch for the phases is 50526 MJD. *C* relates to the observed excitations formed from COMB2016 (Ratcliff and Gross, 2017), *I* relates to ITRF2014 polar motion series (Altamimi *et al.*, 2016), *J* relates to JTRF2014 and *D* to DTRF2014. Parenthesised entries are formal errors (1-sigma level).

Seasonals - Observed (Kouba, 2005) vs GFZ χ

- PM rate observations have been used to construct the observed $\tilde{\chi}$

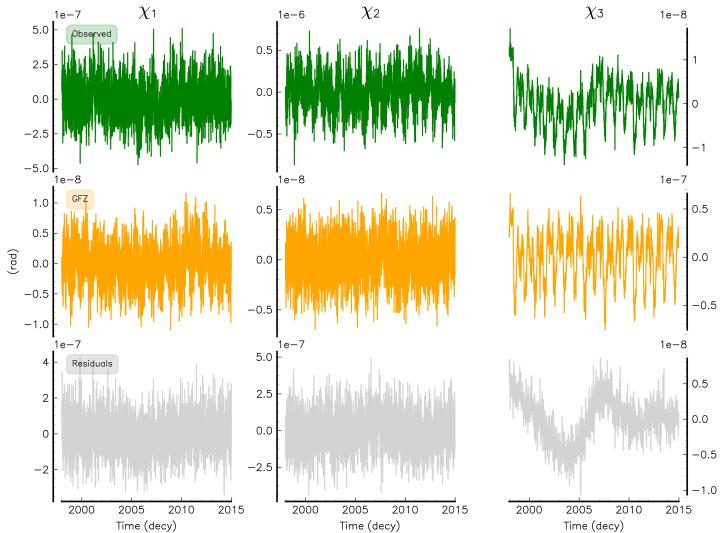
	Annual				Semi-Annual			
	Prograde		Retrograde		Prograde		Retrograde	
	A (uas)	φ (deg)	A (uas)	φ (deg)	A (uas)	φ (deg)	A (uas)	φ (deg)
Observed Excitation (1998.0-2015.0)								
<i>C</i>	17568.3 (409.7)	114.3 (1.3)	10818.1 (409.7)	52.2 (1.8)	2885.2 (409.6)	106.2 (8.1)	4082.4 (409.6)	124.5 (7.6)
<i>I</i>	20270.7 (429.7)	123.1 (1.2)	11839.8 (429.7)	60.4 (1.6)	2500.4 (429.5)	101.0 (9.8)	4488.8 (429.5)	133.8 (8.9)
<i>J</i>	20261.7 (429.6)	122.8 (1.2)	11733.9 (429.5)	60.5 (1.6)	2528.4 (429.4)	102.7 (9.7)	4529.6 (429.4)	132.9 (8.8)
<i>D</i>	20506.5 (441.5)	123.0 (1.2)	11920.4 (441.5)	60.9 (1.6)	2729.2 (441.4)	100.2 (9.3)	4359.9 (441.4)	132.1 (8.5)
Total Geophysical Excitation (1998.0-2015.0)								
<i>T</i>	17378.5 (448.0)	116.6 (1.5)	8762.3 (448.0)	59.3 (2.2)	823.1 (447.8)	106.4 (31.2)	1559.5 (447.8)	171.3 (29.2)

Amplitudes are in *uas* (microarcseconds) and phases are given in decimal degrees. The reference epoch for the phases is 50526 MJD. *C* relates to the observed excitations formed from COMB2016 (Ratcliff and Gross, 2017), *I* relates to ITRF2014 polar motion series (Altamimi *et al.*, 2016), *J* relates to JTRF2014 and *D* to DTRF2014. Parenthesised entries are formal errors (1-sigma level).

Analyses of the differences

$(\tilde{\chi}_{OBS} - \chi_{GFZ})$ in the time domain

$(\tilde{\chi}_{JTRF} - \chi_{GFZ})$ - With Observed Polar Motion Rates



Variance Reduction

Variance Reduction is computed as

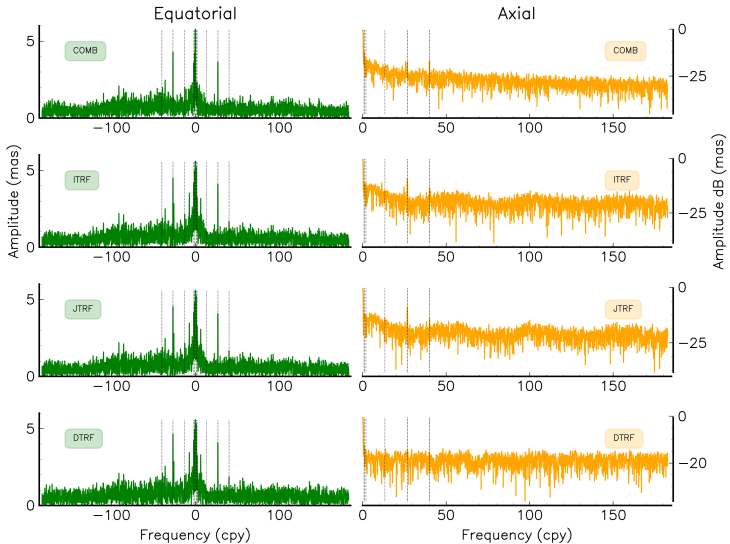
$$\frac{\text{Var}[\chi_i] - \text{Var}[r_i]}{\text{Var}[\chi_i]} \cdot 100$$

where Var is the Variance operator, and r_i is the i -th component of the residual excitation series (after removal of the GFZ EAM).

	χ_1	χ_2	χ_3
Only observed PM, à la Wilson and Chen (1996)			
\mathcal{C}	44.959	67.468	71.429
\mathcal{I}	46.856	68.800	55.184
\mathcal{J}	46.792	68.784	59.118
\mathcal{D}	44.959	67.468	71.429
Observed PM and PM Rates, à la Kouba (2005)			
\mathcal{C}	47.840	69.012	71.449
\mathcal{I}	45.192	70.339	55.218
\mathcal{J}	45.759	70.409	59.152
\mathcal{D}	42.401	68.628	65.017

**Analyses of the differences
($\tilde{\chi}_{OBS} - \chi_{GFZ}$) in the frequency
domain**

Amplitude Spectra of $(\tilde{\chi} - \chi_{GFZ})$ - Kouba (2005)



Median Amplitudes of $\mathcal{F}(\tilde{\chi} - \chi_{GFZ})$ by Spectral Bands

< 0.1 cpy		0.1 – 1 cpy		1 – 2 cpy		2 – 53 cpy		53 – 180 cpy		
Prograde	Retrograde	Prograde	Retrograde	Prograde	Retrograde	Prograde	Retrograde	Prograde	Retrograde	
Wilson and Chen (1996)										
\mathcal{C}	5.301 (7.504)	5.776 (8.169)	1.563 (0.971)	1.746 (1.572)	1.749 (0.481)	1.890 (0.874)	0.603 (0.389)	0.821 (0.480)	0.515 (0.272)	0.571 (0.314)
\mathcal{I}	5.271 (7.461)	5.752 (8.135)	1.560 (0.965)	1.734 (1.563)	1.742 (0.478)	1.891 (0.865)	0.600 (0.387)	0.823 (0.479)	0.502 (0.265)	0.553 (0.312)
\mathcal{J}	5.269 (7.459)	5.747 (8.128)	1.561 (0.965)	1.736 (1.563)	1.742 (0.477)	1.894 (0.867)	0.602 (0.387)	0.823 (0.479)	0.504 (0.265)	0.555 (0.312)
\mathcal{D}	5.266 (7.454)	5.747 (8.127)	1.560 (0.964)	1.735 (1.564)	1.742 (0.478)	1.893 (0.866)	0.596 (0.386)	0.824 (0.479)	0.506 (0.265)	0.555 (0.312)
Kouba (2005)										
\mathcal{C}	5.261 (7.447)	5.759 (8.145)	1.529 (0.952)	1.700 (1.556)	1.739 (0.483)	1.861 (0.847)	0.608 (0.389)	0.873 (0.479)	0.510 (0.260)	0.575 (0.328)
\mathcal{I}	4.886 (6.922)	5.593 (7.910)	1.814 (1.180)	1.669 (1.414)	1.968 (1.212)	2.038 (0.985)	0.643 (0.478)	0.904 (0.550)	0.526 (0.273)	0.578 (0.332)
\mathcal{J}	4.975 (7.047)	5.598 (7.917)	1.779 (1.210)	1.684 (1.372)	1.978 (1.223)	1.971 (0.951)	0.647 (0.473)	0.907 (0.546)	0.524 (0.272)	0.574 (0.332)
\mathcal{D}	4.601 (6.519)	5.542 (7.838)	1.868 (1.191)	1.680 (1.445)	2.102 (1.231)	2.027 (0.955)	0.696 (0.478)	0.941 (0.562)	0.589 (0.304)	0.629 (0.349)

\mathcal{C} relates to the observed excitations formed from COMB2016, \mathcal{I} relates to the ITRF2014 EOP series, \mathcal{D} relates to the DTRF2014 EOP series. Each row contains median spectral values along with their standard deviations (in parentheses) computed within each spectral band. Units are *mas* (milliarcsecond).

Analysis of the Spectral Coherence between $\tilde{\chi}$ and χ_{GFZ}

Cross Spectrum $\mathcal{R}(\omega)$ and Spectral Coherence $\rho(\omega)$

The cross spectrum between complex-valued sequences x and y is defined to be

$$\mathcal{R}(\omega) = \frac{S_{xy}(\omega)}{\sqrt{S_{xx}(\omega) \cdot S_{yy}(\omega)}}$$

where

- S_{xy} is an adaptive multi-tapered estimate of the cross spectrum between x and y
- $S_{xx}(\omega)$ and $S_{yy}(\omega)$ are adaptive multi-tapered estimate of the spectral density function of x and y , respectively

$\mathcal{R}(\omega)$ is a complex-valued function of the frequency whose squared module

$$\rho(\omega) = \frac{|S_{xy}^2(\omega)|}{S_{xx}(\omega) \cdot S_{yy}(\omega)} \in [0, 1]$$

is generally referred to as **spectral coherence**

Median Spectral Coherences by Spectral Bands

	< 0.1 cpy		0.1 – 0.3 cpy		0.3 – 1 cpy		1 – 2 cpy		2 – 12.175 cpy		12.175 – 24.35 cpy		24.35 – 36.25 cpy		36.25 – 121.75 cpy		121.75 – 183.0 cpy	
	Prograde	Retrograde	Prograde	Retrograde	Prograde	Retrograde	Prograde	Retrograde	Prograde	Retrograde	Prograde	Retrograde	Prograde	Retrograde	Prograde	Retrograde	Prograde	Retrograde
Wilson and Chen (1996)																		
<i>C</i>	0.724	0.723	0.728	0.728	0.731	0.721	0.735	0.730	0.850	0.827	0.862	0.896	0.784	0.877	0.583	0.372	0.120	0.366
<i>I</i>	0.725	0.724	0.728	0.728	0.732	0.721	0.735	0.730	0.850	0.827	0.862	0.897	0.792	0.878	0.622	0.386	0.300	0.437
<i>J</i>	0.725	0.724	0.728	0.728	0.732	0.721	0.735	0.730	0.850	0.827	0.862	0.897	0.792	0.877	0.621	0.387	0.296	0.435
<i>D</i>	0.725	0.724	0.728	0.728	0.732	0.721	0.736	0.730	0.850	0.827	0.862	0.897	0.793	0.878	0.618	0.386	0.289	0.425
Kouba (2005)																		
<i>C</i>	0.725	0.723	0.728	0.728	0.732	0.721	0.736	0.730	0.850	0.827	0.862	0.895	0.784	0.877	0.577	0.371	0.033	0.270
<i>I</i>	0.721	0.719	0.724	0.719	0.725	0.702	0.735	0.709	0.791	0.738	0.835	0.875	0.766	0.860	0.487	0.361	0.073	0.391
<i>J</i>	0.720	0.718	0.724	0.720	0.724	0.703	0.733	0.710	0.795	0.742	0.835	0.875	0.767	0.861	0.485	0.363	0.078	0.391
<i>D</i>	0.737	0.735	0.741	0.735	0.742	0.716	0.753	0.715	0.782	0.740	0.828	0.873	0.758	0.833	0.347	0.299	0.042	0.257

C relates to the median spectral coherences between COMB2016 and GFZ excitations, *I* relates to those between ITRF2014 and GFZ, *J* relates to the median spectral coherences between JTRF2014 and GFZ, *D* relates to those between DTRF2014 and GFZ. Cross spectra adopted in these analyses are characterized by a bandwidth of 1.9 cpy. The 95% level of confidence associated with these spectra is 0.09.

Conclusions - Intra-Comparisons

- **Seasonal (Differences to COMB)**

Evidence of corruption of PM signal frequencies from all 3 combination centers. Corruption is the highest for JTRF- y_p annual amp (18.36 uas), followed by ITRF- x_p annual amp (9.27 uas).

- **TCH**

ITRF-EOP uncertainties are on the whole the smallest, JTRF-EOPs provide intermediate results.

DTRF- y_p provide the smallest PM uncertainty (14.15 uas).

DTRF-EOP rate uncertainties are one order of magnitude larger (adoption of satellite-derived LOD in DTRF combination may be implicated)

- **Bayesian Inversions in the Spectral Domain**

PM noise structure adequately described by AR[1] with $\varphi \sim 1$ (random walk).

JPL-COMB PM characterized by the largest high-frequency noise (22.15 uas).

DTRF PM has the lowest noise (17.96 uas).

Maximum differences in the noise amplitudes in the order of ≈ 4 uas (unlikely to be statistically significant).

Conclusions - Inter-Comparisons in the Excitation Domain

- **Seasonal Terms (Differences to χ_{GFZ})**

Largest signal consistency is found for the annual prograde amplitude.

Although, the amplitude differences are fairly large and in the order of 200 uas. ($\tilde{\chi}_{COMB}$ is the closest to χ_{GFZ}).

Annual retrograde and semi-annual signals are markedly different.

The use of PM observed rates when forming the geodetic χ is still problematic and causes large corruptions to the seasonal signals (in amplitude).

Yet, we found evidences of an increased variance reduction when PM rates are used

- **Differences ($\tilde{\chi} - \chi_{GFZ}$) in the frequency domain**

Spectral analyses suggest that most of the variance reduction occurs at lower frequencies (< 1 cpy), whereas PM rates produce the highest corruption at higher frequencies.

- **Analyses of Spectral Coherence ($\tilde{\chi}, \chi_{GFZ}$)**

The observed \tilde{chi} from ITRF, JTRF, and DTRF appear to be identically correlated to χ_{GFZ} .

Spectral Coherence are in the order of 0.7 – 0.8 within the band 0 – 36.25 cpy.

For $\tilde{\chi}_{DTRF}$ only, the adoption of observed PM rates produces slightly increased coherences at low frequencies (< 1.0 cpy), whereas there is evidence of significant loss of correlation at higher frequencies. (parameter correlations to satellite-derived LOD may be implicated).

References

- Altamimi, Z., Rebischung, P., Métivier, L., and Collilieux, X. (2016). ITRF2014: A new release of the International Terrestrial Reference Frame modeling nonlinear station motions. *J Geophys Res-Sol Ea*, **121**(8), 6109–6131.
- Barnes, R. T. H., Hide, R., White, A. A., and Wilson, C. A. (1983). Atmospheric angular momentum fluctuations, length-of-day changes and polar motion. *P Roy Soc Lond A Mat*, **387**(1792), 31–73.
- Brockwell, P. J. and Davis, R. A. (1986). *Time Series: Theory and Methods*. Springer. Second Edition.

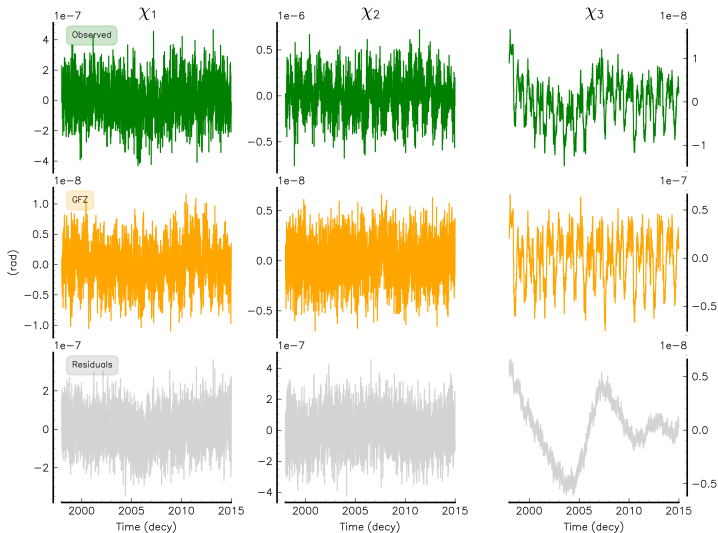
- Dobslaw, H. and Dill, R. (2018). Predicting Earth orientation changes from global forecasts of atmosphere-hydrosphere dynamics. *Adv Space Res*, **61**(4), 1047–1054.
- Gross, R. S., Eubanks, T. M., Steppe, J. A., Freedman, A. P., Dickey, J. O., and Runge, T. F. (1998). A Kalman-filter-based approach to combining independent Earth-orientation series. *J Geodesy*, **72**(4), 215–235.
- Kouba, J. (2005). Comparison of polar motion with oceanic and atmospheric angular momentum time series for 2-day to Chandler periods. *J Geodesy*, **79**(1-3), 33–42.
- Premoli, A. and Tavella, P. (1993). A Revisited Three-Cornered Hat Method For Estimating Frequency Standard Instability. *IEEE Trans Instrum Meas*, **42**(1), 7–13.

- Ratcliff, J. T. and Gross, R. S. (2017). Combinations of Earth Orientation Measurements: SPACE2016, COMB2016 and POLE2016. JPL Publication 17-8.
- Ray, J., Kouba, J., and Altamimi, Z. (2005). Is there utility in rigorous combination of VLBI and GPS Earth orientation parameters? *J Geodesy*, **79**, 505–511.
- Rebischung, P., Ray, J., and Chen, W. (2017). A Comparison of ITRF2014, DTRF2014, and JTRF2014 Polar Motion Series with Geophysical Excitation Data. In *Vol. 19, EGU2017-8234 Geophysical Research Abstracts*. European Geosciences Union 2017.
- Seitz, M., Bloßfeld, M., Angermann, D., Schmid, R., Gerstl, M., and Seitz, F. (2016). The new DGFI-TUM realization of the ITRS: DTRF2014 (data).

Wilson, C. R. (1985). Discrete polar motion equations. *Geophys J Int*, **80**(2), 551–554.

Wilson, C. R. and Chen, J. (1996). Discrete polar motion equations for high frequencies. *J Geodesy*, **70**(9), 581–585.

SG-GFZ Excitations - KEOF - Kouba (2005)



Seasonal Amplitudes - GFZ Excitations

$$\chi = \chi_1 + i\chi_2 = A_p e^{i(\phi_p + \omega t')} + A_r e^{i(\phi_r - \omega t')}$$

	Annual				Semi-Annual			
	Prograde		Retrograde		Prograde		Retrograde	
	A	φ	A	φ	A	φ	A	φ
Atmosphere								
\mathcal{P}	16530.6 (120.2)	-25.3 (0.4)	16244.2 (120.2)	178.9 (0.4)	2032.7 (120.1)	-164.1 (3.4)	4076.9 (120.1)	-44.7 (2.3)
\mathcal{M}	4267.3 (113.3)	77.3 (1.5)	2641.2 (113.3)	-29.8 (2.1)	1074.0 (113.3)	168.9 (6.0)	726.1 (113.3)	69.1 (7.5)
Ocean								
\mathcal{P}	2340.0 (119.0)	91.7 (2.9)	2312.4 (119.1)	-6.8 (3.3)	1072.3 (119.1)	0.1 (6.4)	1261.3 (119.1)	60.2 (5.2)
\mathcal{M}	2364.8 (152.8)	61.0 (3.7)	3026.6 (152.8)	-74.2 (3.3)	1574.9 (152.8)	-35.3 (5.6)	2047.5 (152.8)	97.6 (4.7)
Continental Water Surface								
\mathcal{P}	3409.4 (69.8)	99.0 (1.2)	8639.4 (69.8)	64.6 (1.1)	781.5 (69.8)	-71.1 (5.1)	1053.2 (69.8)	-145.3 (5.3)
\mathcal{M}	2.9 (0.0)	-153.7 (0.9)	1.9 (0.0)	-164.4 (1.0)	3.4 (0.0)	-123.9 (0.8)	3.5 (0.0)	-137.8 (0.7)
Sea Level								
\mathcal{P}	1751.6 (10.3)	-145.1 (0.3)	1751.6 (10.3)	-99.2 (0.3)	248.2 (10.3)	-139.5 (2.4)	248.2 (10.3)	-104.8 (2.1)
Total Geophysical Excitation								
	15476.3 (293.2)	14.4 (1.1)	7640.3 (293.2)	165.6 (1.9)	2240.6 (293.2)	-105.3 (7.5)	2586.2 (293.0)	2.1 (8.3)

Amplitudes are in *uas* (microarcseconds) and phases are given in decimal degrees. The rows \mathcal{P} gather estimates for the pressure component of the EAM, whereas rows \mathcal{M} relate to the motion terms. The reference epoch for the phases is 50526 MJD. Parenthesised entries are formal errors (1-sigma level).

Confidence Level on Spectral Coherence

$$c(\alpha) = \frac{\mathcal{F}_{2,df-2}(\alpha)}{\frac{df}{2} - 1 + \mathcal{F}_{2,df-2}(\alpha)}$$

where

- α is the confidence level
- df , degree of freedom, $df = 2 \cdot NW$, where NW is the time-bandwidth product parameter adopted in the multitapered spectral estimation
- \mathcal{F} is the inverse of the cumulative Fisher distribution

$c(\alpha)$ can be used

- to test the null hypothesis, i.e. absence of coherence/spectral correlation between two series
- to establish a threshold above which there exists statistically significant spectral coherence